Engineering Solid Mechanics 9 (2021) 137-152

Contents lists available at GrowingScience

Engineering Solid Mechanics

homepage: www.GrowingScience.com/esm

Effect of titanium alloy powder reinforcement on the mechanical properties and microstructural evolution of GMAW mild steel butt joints

T.N. Odiaka[a*], S.A. Akinlabi[b], N. Madushele[a], S. Hassan[b], and E.T. Akinlabi[c]

[a]*Department of Mechanical Engineering Science, University of Johannesburg, Johannesburg, South Africa*
[b]*Department of Mechanical Engineering, Walter Sisulu University, Butterworth Campus, Butterworth, South Africa*
[c]*Pan African University for Life and Earth Sciences Institute, Ibadan, Nigeria*

ARTICLEINFO

Article history:
Received 10 October2020
Accepted 17 December 2020
Available online
17 December 2020

Keywords:
GMAW
Mild Steel
Taguchi
DoE
Microstructural Evolution

ABSTRACT

Despite its well-reported application in a few welding processes, the use of reinforcing powders in weld joints to improve weld integrity has not garnered ample research attention for Gas Metal Arc Welding (GMAW) process. In this study, the adoption of Titanium alloy powders as metallic reinforcement for mild steel butt welds was investigated. By adopting Taguchi's L4 orthogonal array, process optimisation for titanium-reinforced mild steel butt welds were first carried out. In the second phase of welding, the optimum parameters were used to create and compare two sets of weldments; one set was reinforced with titanium alloy powder and the other set left unreinforced. It was observed that in the Weld Metal (WM) region, the titanium-reinforced samples had higher micro-hardness values than their unreinforced counterparts with an average of 285.62 HV and 211.6 HV respectively. However, there was no substantial improvement in the ultimate tensile strength of the mild steel butt welds due to titanium powder reinforcements. Interestingly, the formation of acicular ferrite microstructure was more prevalent in the titanium-reinforced weldments and this was attributed to the presence of titanium inclusions in the weld metal. This prevalence of acicular ferrite suggests improved toughness properties in the weld joint region. While the higher hardness values in the Weld Metal of the reinforced sample indicates improved wear resistance.

1. Introduction

There is a widespread use of Gas Metal Arc Welding (GMAW) to join materials in the metal industry. This is largely due to its high weld quality, ease of use, reduced distortion, high metal deposition rate, amongst others (Hooda et al., 2012). GMAW involves the joining of metals by establishing an electric arc between the materials and an electrode to induce melting while the molten electrode is deposited into the weld pool. This solidifies upon cooling, resulting in a permanent fusion of the materials. An inert gas, usually argon, helium, CO_2 or a combination of these is supplied to protect the weld pool from contamination (Kazi et al., 2015; Pal, 2015). GMAW is also one of the most extensively used welding processes for joining mild steel. Mild steel has diverse applications in cookware, machine-ware and construction due to its good malleability and weldability (Kumar et al., 2016). The complicated physics involved in welding, such as phase change, metal deposition, inhomogeneous heating and cooling rates

* Corresponding author. Tel: +2348105298770
E-mail addresses: nkemodiaka@gmail.com (T.N. Odiaka)

doi: 10.5267/j.esm.2020.12.005

result in the compromise of the structural integrity of weld joints. Consequently, substantial research has gone into improving the weld integrity of steel welds in general (Odiaka et al. 2018). Optimisation of parameters using Taguchi's Design of Experiments (DoE), Response Surface Methodology (RSM), Artificial Neural Network (ANN) and etc. have been employed by numerous scholars to improve the mechanical properties and welding quality of fusion welded and solid state welded joints made of steel, aluminium, titanium and other alloys (Rakesh, 2014; Sapakal & Telsang, 2012; Singh, 2013; Srivastava & Garg, 2017; Utkarsh et al., 2014; Owunna & Ikpe 2019;Akbari et al. 2019; Aita et al. 2020; Shojaeefard et al. 2014; Eslami et al. 2019; Torabi et al. 2018; Narasimharaju & Sankunny 2019; Aliha et al. 2016, 2017, 2019, 2020; Zhao et al. 2017;Taheri-Behrooz et al. 2018; Mohammad Aliha et al. 2018; Lacki & Derlatka 2017; Olabi et al. 2006; Sivagurumanikandan et al. 2018; Anand et al. 2015; Jacques & El Ouafi 2018; Narendranath & Chakradhar 2018). Post Weld Heat Treatment (PWHT) methods are also typically applied to aid grain refinement and improve mechanical properties of weldments (Ramakrishna et al., 2016).

The use of powder reinforcement in welding has also become an area of interest. However, this seems to be more prominent in Friction Stir Welding (FSW). Pantelis et al. (2016) reinforced Friction Stir Welded AA5083-H111 and AA6082-T6 Aluminium alloys with SiC Nano-particles and observed grain refinement resulting in higher hardness and ultimate tensile strength than in the unreinforced weldments. Other authors have also used SiC Nano-particle reinforcement in FSW of other aluminium alloys and reported improvement in weldment properties (Bahrami et al., 2014; Byung-Wook, et al., 2012). Particle reinforcement in Gas Tungsten Arc Welding of aluminium alloys has been reported by Fattahi et al. (2015), where TiC Nano-particle reinforced aluminium fillers were used. The improvement of the mechanical properties of the aluminium weldment was reportedly due to grain refinement stimulated by the uniformly distributed TiC nanoparticles. Other particle reinforcements such as B_4C, Al2O3 and TiO have been used in FSW of aluminium alloys (Mirjavadi et al., 2017; Paidar et al., 2018; Yuvaraj & Aravindan, 2015).

Powder reinforcements have been applied in Submerged Arc Welding (SAW) of mild steel by Singh et al. (2016). CaF_2, FeMn and NiO were added in varying amounts to welding fluxes. CaF_2 and FeMn were reported to be significant in improving the impact toughness of the weldment. Nickel is known to improve the impact toughness of steel welds due to acicular ferrite formation (da Trindade Filho et al., 2004). Ana et al. (2009) reported the significance of titanium particles in the formation of acicular ferrite in steel welds during SAW. Mn also promotes hardness and strength in steel welds to a certain degree, such that very high Mn content could result in weld embrittlement (Singh et al., 2016).

There appears to be a very little study in literature, if any, focusing on particle reinforcement in mild steel welds using the GMAW process. This study investigates the effect of titanium alloy powder reinforcement on the mechanical properties and microstructures of mild steel butt joint weldments. Titanium reinforced mild steel welds were first optimized using an L4 Taguchi orthogonal array. The optimized weldments were then compared with unreinforced mild steel weldments and tested for hardness and tensile strength. Titanium was selected as a reinforcement of choice due to its high tensile strength and hardness properties.

2. Materials and Experimental Methodology

2.1 Materials

The parent material welded in this study is hot rolled AISI 1008 mild steel and its chemical composition is presented in Table 1. Similarly, Table 2 also presents the chemical composition of the ER 70S-6 1.2 mm thick electrode used during the GMAW welding process. The mild steel sheets were machined into dimensions of 100 × 40 × 3 mm. A 45^0 chamfer was machined at the edge of each sheet, creating a groove where the two sheets are joined together. This groove was filled with titanium powder reinforcement as shown in Fig. 1.

Table 1. Chemical composition of Parent Material, AISI 1008

Elements	*C*	*Si*	*Mn*	*P*	*S*	*Cr*	*Mo*	*Ni*	*Al*	*Fe*
% by wt.	0.072	0.068	0.320	0.0098	0.0091	0.042	0.0050	0.0064	0.042	Balance

Table 2. Chemical composition of ER 70S-6 wire electrode

Elements	*C*	*Mn*	*Si*	*Cu*	*Fe*
% by wt. (Max)	0.15	1.85	1.15	0.5	Balance

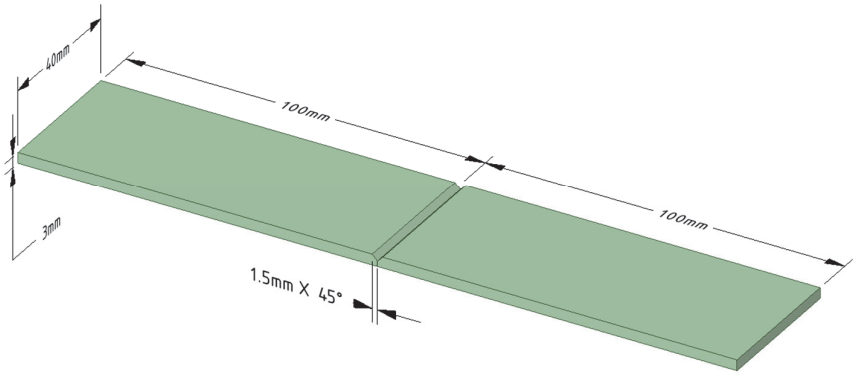

Fig. 1. Schematic of Butt Joint configuration

In the first stage of the welding, which was the optimisation stage, two titanium reinforcement powders were selected; commercially pure titanium and Ti 6-2-2-2-2 alloy powder. The morphology of both powders obtained from SEM is shown in Fig. 2. Scanning Electron Micrographs of (a) Commercially pure titanium (b) Ti 6-2-2-2-2 alloy powder. Fig. 2 shows both powders to be spherical with their average particle sizes ranging from ≈ 40.54µm to 95.12µm and ≈19.88µm to 83.34µm for commercially pure titanium and Ti 6-2-2-2-2 alloy respectively. Ti 6-2-2-2-2 was selected for its high strength and fracture toughness properties while commercially pure titanium is known for its ductility.

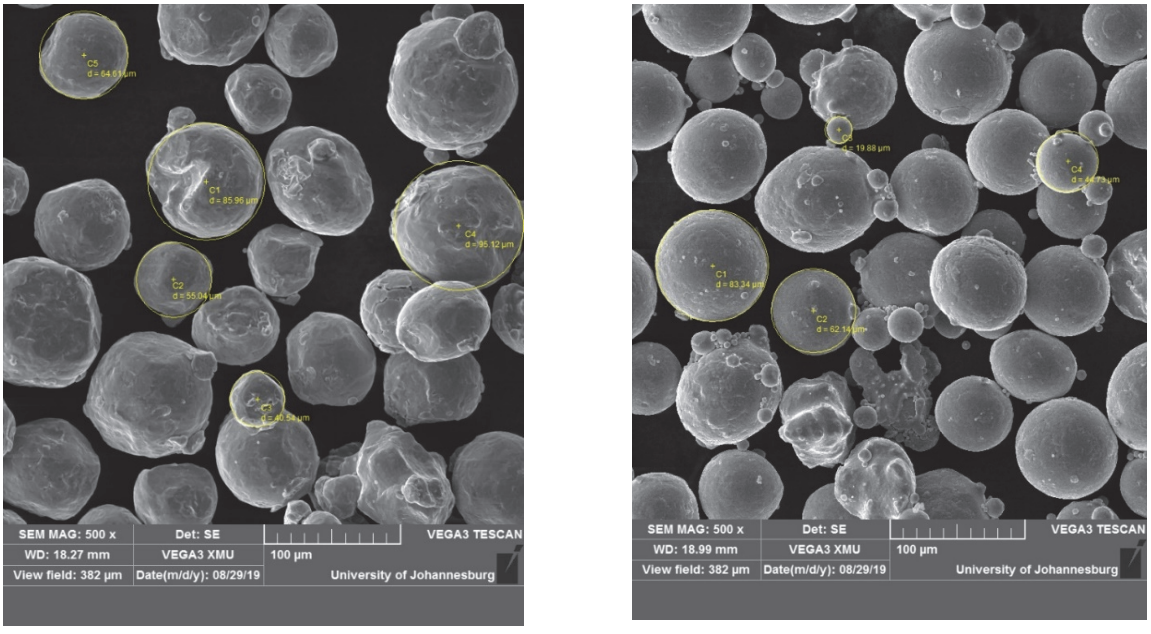

(a) **(b)**

Fig. 2. Scanning Electron Micrographs of (a) Commercially pure titanium (b) Ti 6-2-2-2-2 alloy powder

2.2 Experimental Procedure

In the first welding phase, the butt welds were first optimized using Taguchi's L4 Orthogonal Array. Taguchi's Design of Experiment (DoE) method is a statistical tool employed to study the effect of several process parameters on desired output responses. This is achieved by using predefined orthogonal arrays which determine experimental runs for selected factors and their respective values. By using signal-to-noise (S/N) ratios, optimum process parameters were obtained for the experiment. Signal-to-noise ratios are derived from loss functions and are a measure of the desirability of the output response per experimental run. For this study, the weldments were optimized for tensile strength. Consequently, a larger-is-better S/N ratio loss function was adopted and is given in Eq. (1).

$$[S/N]_l = -10.\log_{10}\left[\frac{\sum\frac{1}{\mu^2}}{n}\right] \quad (1)$$

where μ represents the output mean, while n represents the number of runs.

From consultation with welding handbooks, and initial pilot runs, the welding parameters were selected and are presented as the design matrix in Table 3. The adopted L4 orthogonal array is presented in Table 4 and the parametric combinations for each experimental run are also presented.

Table 3. Design Matrix for Welding Experiment.

Factors	Voltage	Current	Reinforcement
Level 1	22	120	Cp. Titanium Powder
Level 2	22	130	Ti 6-2-2-2-2 alloy Powder

Table 4. L4 Orthogonal Array with Process Parameter Values

Experiments	Voltage (V)	Current (A)	Reinforcement
B1	22	120	Cp. Titanium Powder
B2	22	130	Ti 6-2-2-2-2 alloy Powder
B3	24	120	Ti 6-2-2-2-2 alloy Powder
B4	24	130	Cp. Titanium Powder

The welding experiment was conducted using a constant voltage, semi-automatic Miller XMT-400 series GMAW machine at the South African Institute of Welding, Johannesburg, South Africa. Each mild steel workpiece was well aligned and clamped. The titanium powder reinforcement was introduced to fill the groove before welding began. Besides the varied welding parameters, the gas flow rate was kept constant at 15 lpm while travel speed was kept at an average of 24 cm/min. As is the recommendation whilst using Taguchi's DoE, the welding runs were done randomly.

The weldments were cut into shape for tensile strength testing, using the ASTM E8/E8M-16a (ASTM International, 2016) testing standard and tested on a Zwick Roell 2250 Ultimate Testing machine. Samples of the weldments were also cut, mounted and ground for Vickers hardness testing and polished for optical microscopy. In order to reveal the microstructure, the samples were etched with 3% Nital.

At the end of the optimisation phase of the welding experiment, the optimum parameters were reviewed and adopted for the second welding phase. In the second welding phase, a set of weldments were reinforced with titanium powder and another set left unreinforced. The weldments were tested for tensile strength and Vickers hardness as was done in the optimisation phase. Optical microscopy, X-Ray Diffraction Analysis (XRD) and Scanning Electron Microscopy (SEM) with Energy Dispersive Spectroscopy (EDS) were used to characterise the microstructures and conduct failure analysis of the optimised weldments.

3. Results and Discussions

The results are presented in two stages. First, the mechanical properties and microstructure obtained in the optimisation phase are discussed. In the second phase, a direct comparison between the optimised reinforced butt joints and their unreinforced counterparts is discussed vis a vis their mechanical properties and microstructures.

3.1 First Welding Stage: Process Optimisation

3.1.1 Microhardness Profiling

The hardness values typically vary across the weld zones of a weld joint. Consequently, a microhardness profile best describes the hardness of the weld joint. Fig. 3 gives the hardness profiles of the butt joints in the first welding stage.

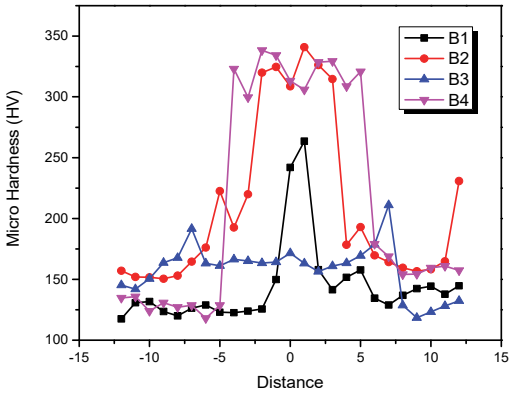

Fig. 3. Vickers Hardness Profiles (First Welding Stage).

Samples B2 and B4 have the highest hardness values in the Weld Metal (WM) within the range of 220-350 HV. Both samples were welded with a current of 130 A. Samples B1 and B3 have much lower hardness values in the WM, particularly sample B3, whose hardness value slightly increases in the heat affected zone (HAZ) and reduces in the WM. B1 and B3 were welded with a lower current of 120A. This suggests a possible role of Current in the hardness values of the WM. However, a study of the microstructures gives a clearer explanation for the non-uniform hardness behaviour of the weldments.

3.1.2 Microstructures

The microstructures of the butt joints samples obtained in the first welding stage are shown in Fig. 4 as obtained via optical microscopy. In the WM region of samples B1 and B3, coarse ferrite grains are observed, and this could explain the low microhardness values observed for these samples in Fig. 3. In Samples B2 and B4, where higher hardness values were obtained, finer grains are observed. Hardness has been reported to be inversely proportional to grain size (Abbaschian & Reed-Hill, 2008). Larger grain sizes also reduce the ductility of a material, as dislocations move more easily in larger grains (Gharibshahiyan et al., 2011). The fine grains formed in the WM of B2 and B4 which includes predominantly acicular ferrite is typically associated with good tensile properties in the WM (Bhadeshia, & Honeycombe, 2006). In the HAZ of samples B2, B3 and B4, widmanstatten and allotriomorphic ferrite are prominent in the coarse grains. The coarse grains observed in the HAZ also explain the lower hardness values typically obtained in this region. Samples B2, B3 and B4 also contain darker degenerate pearlite regions in the HAZ. This is not as pronounced in sample B1, which contains mainly widmanstatten and allotriomorphic ferrite.

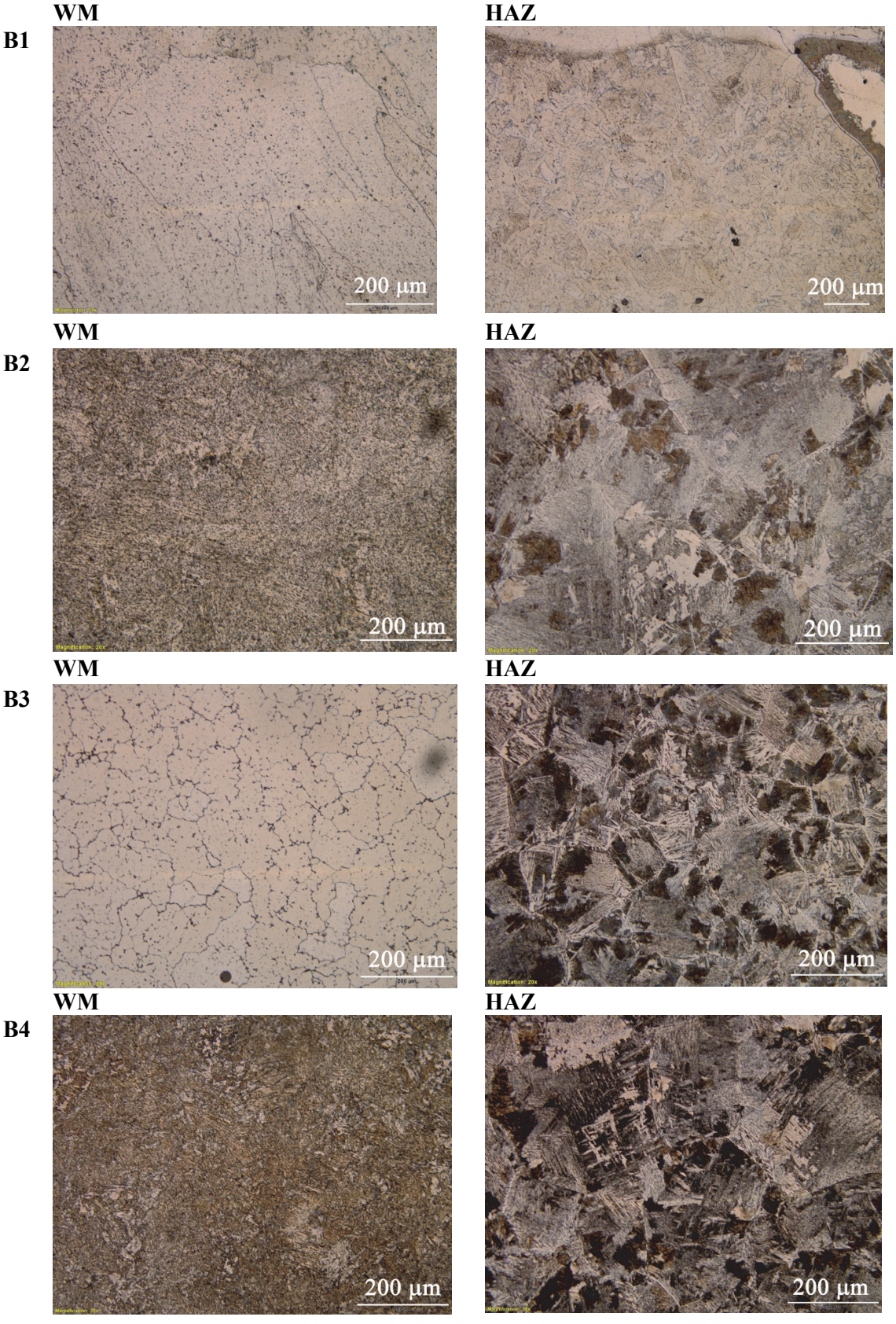

Fig. 4. Microstructure of Butt Welds in the WM and HAZ (20× Magnification)

3.1.3 Tensile Strength Results

The average tensile strengths of the butt joints are presented in Table 5 with their corresponding S/N ratios. Sample B2 gives the highest UTS of 392.81 MPa while sample B1 gives the lowest UTS of 322.59 MPa.

Table 5. Response Table for Ultimate Tensile Strength of Butt Joints.

Weld Number	Voltage (V)	Current (A)	Powder Reinforcement	Avg. UTS (MPa)	S/N Ratio
B1	22	120	Pure Titanium	322.59	50.01
B2	22	130	Ti 6-2-2-2-2	392.81	51.64
B3	24	120	Ti 6-2-2-2-2	355.50	50.99
B4	24	130	Pue Titanium	365.45	51.25

The response table for the S/N ratios at each level for each factor is presented in Table. **6**. It ranks current as the most significant welding parameter. Using the data in Table. **6**, the main effects plot is obtained and is used to identify the optimum welding parameters for the reinforced butt joint samples. The main effects plot for Ultimate Tensile Strength is given in Fig. 5.

Table. 6 S/N Ratios Response Table for UTS of Butt Joints

Level	Voltage	Current	Powder
1	50.82	50.50	50.63
2	51.13	51.45	51.62
Delta	0.30	0.95	0.69
Rank	3	1	2

Fig. 5 shows the optimum process parameters to be at 24 V, 130 A and with Ti 6-2-2-2-2 alloy powder.

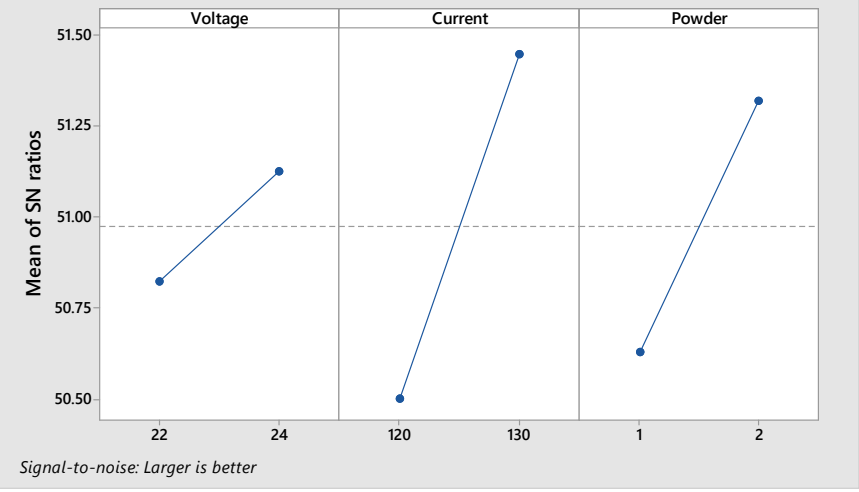

Fig. 5. Main Effects Plot for S/N Ratio of UTS

3.1.4 Failure Mode of Butt Joints

Fig. 6 shows the butt joint samples after failure due to tensile loading. 58% of the butt welds underwent brittle failure at the weld metal region. This indicates poor strength at the weld joint. Micrographs obtained at the fusion zone of samples B1 and B4 depict very large gas pores (Fig. 7). The micrograph of sample B1 also reveals a lack of fusion in the joint.

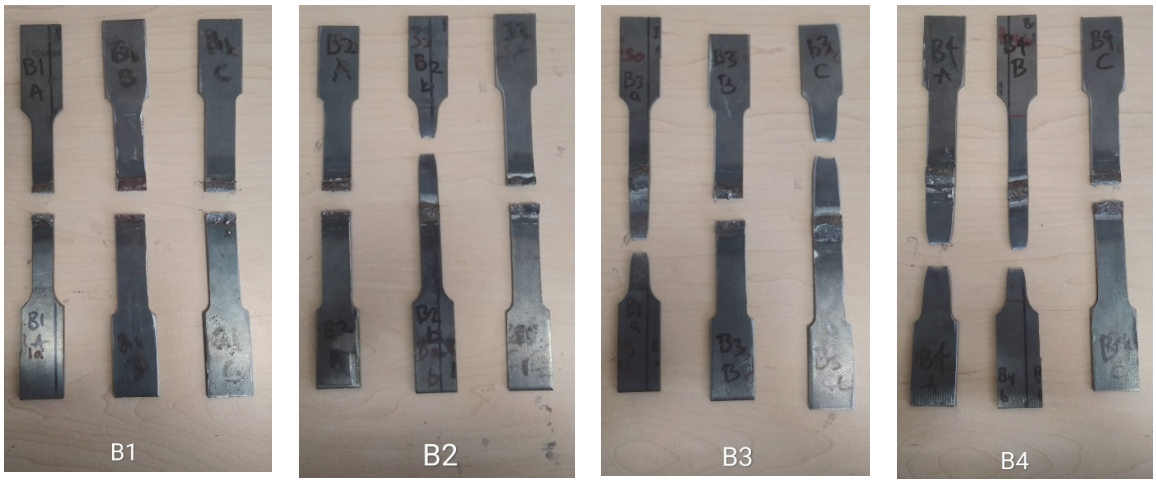

Fig. 6. Failure of Butt Joints due to tensile loading

B1

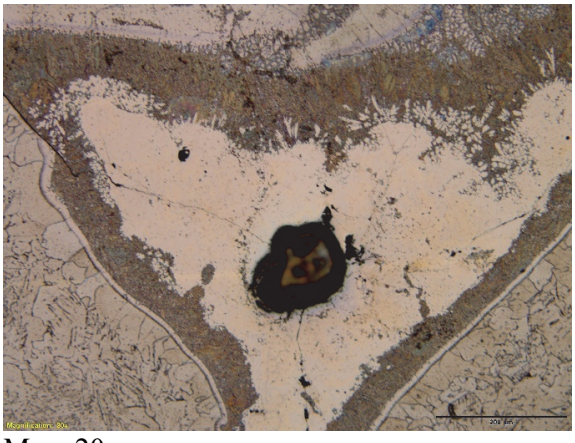

Mag: 20x

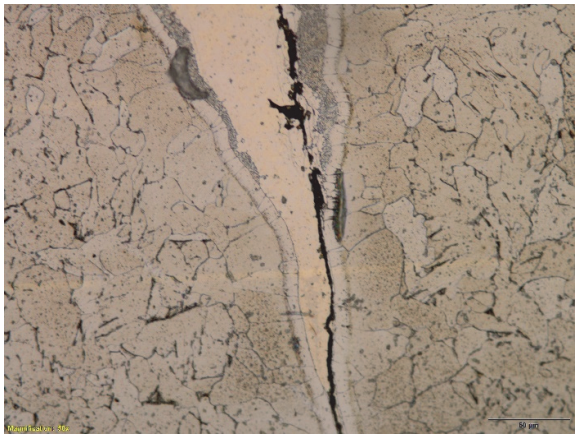

Mag: 50x

B4

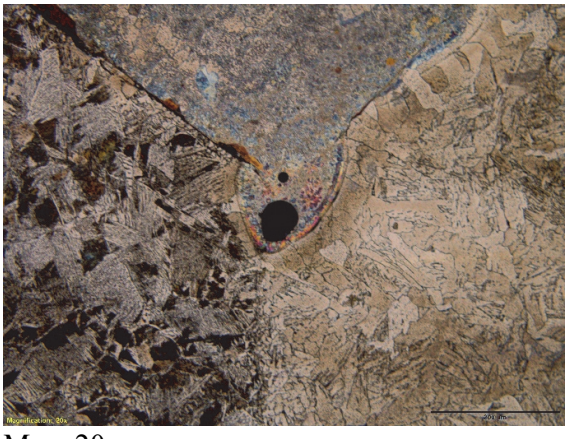

Mag: 20x

Fig. 7. Micrographs of samples B1 and B4

The presence of these large gas pores and lack of fusion in B1 precipitated the need to increase the welding current for the final welding phase. By increasing the welding current, the depth of penetration is expected to improve to ensure proper fusion between the materials. To get rid of the gas pores, subsequent plates used for welding were thoroughly cleaned with acetone to reduce the propensity for gas entrapments during the welding process.

3.2 Final Welding Stage: Direct Comparison

In this stage, optimised welding parameters of 24 V and 220 A were applied to two sets of weldments. The first set was reinforced with Ti 6-2-2-2-2 powder while the other set was left unreinforced. A direct comparison of tensile strength, hardness and microstructural evolution was carried out to determine the effect of titanium alloy powder reinforcement.

3.2.1 Vickers Hardness of Optimised Samples

Fig. 8 shows the micro-hardness profiles of the optimised samples. BP represents the reinforced sample, while BN is the sample with no reinforcement. In the WM region, the hardness is much higher in the reinforced sample, with an average of 285.62 HV compared to an average of 211.6 HV in the unreinforced sample. This increased hardness is attributed to the presence of titanium alloy reinforcement in the WM and a possible formation of intermetallic compounds which is discussed later. The higher hardness in the reinforced sample also suggests improved wear resistance of the reinforced sample as there is a direct relationship wear resistance and microhardness (Sevim & Eryurek, 2006).

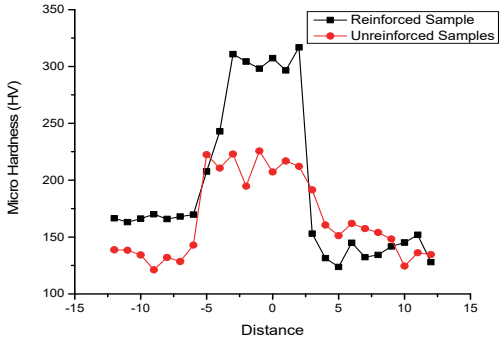

Fig. 8. Microhardness profile of optimised samples

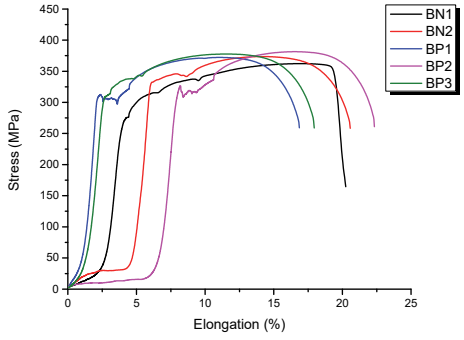

Fig. 9. Tensile strength of optimised samples

3.2.2 Ultimate Tensile Strength

Fig. 9 shows the stress-strain curves of the optimised samples obtained from tensile testing. BN indicates samples without powder reinforcements, while BP represents reinforced samples. It is evident that there is no substantial improvement in the tensile strength of the material due to titanium alloy powder reinforcement. Sample BP2 has the highest UTS with 381.39 MPa whilst sample BN1 with 362.17 MPa has the lowest UTS. The lowest value of the UTS from the reinforced samples was 372.18 MPa. However, one of the unreinforced samples has a UTS 373.56 MPa, which is higher than the lowest strength of one of the reinforced samples. This strengthens the conclusion that the addition of titanium reinforcement cannot be conclusively said to improve the strength of the weld joint. The ductility of all optimised samples ranges from ≈17 to 23 per cent elongation. The joint efficiency of the optimised samples is given in Table 7. The tensile strength of the parent AISI 1008 material was experimentally obtained at 388.46 MPa. The joint efficiency of a welded sample is calculated as the ratio of UTS of the welded sample to the UTS of the parent material. The high joint efficiencies presented in Table 7 indicate good weldability of the selected material. There is a small increase in the average tensile strength of the reinforced sample over the reinforced sample by 9 MPa. However, this 2.4 % increase is not significant enough to conclude on a substantial improvement of the tensile strength of the weldment due to titanium alloy reinforcement.

Table 7. Joint Efficiency of Optimised Samples

Weld Number	Avg UTS (MPa)	Joint Efficiency (%)
BN	367.87	94.64
BP	376.75	96.92

3.2.3 Microstructures

In order to explain the hardness behaviour of the optimised welded samples, it's imperative to consider the microstructural evolution in the WM region. Fig. **10** shows the micrographs of the WM region of the unreinforced and reinforced samples. As is typical with mild steel weldments, a few oxides can be identified. However, what is more notable is the dominance of Allotriomorphic ferrite in the unreinforced sample. Some widmanstatten ferrite is also observable.

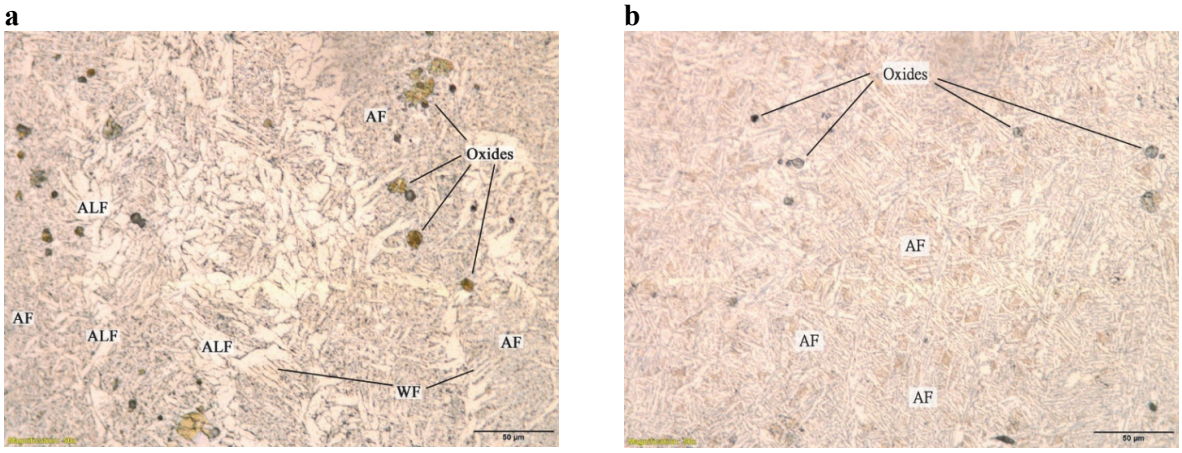

Fig. 10. Micrographs of the weld metal region of (a) Unreinforced sample (b) Reinforced sample

This contrasts with the prevalence of acicular ferrite in the reinforced sample. While there is some acicular ferrite observed in the unreinforced sample, this desirable microstructure is more prevalent in the reinforced sample. Acicular ferrite is typically associated with improved toughness, because of the interlocking nature of its microstructure that inhibits crack propagation and cleavage fracture (Bhole et al., 2006; Mirzaei et al., 2013). The prevalence of acicular ferrite is attributed to the presence of titanium reinforcement. Due to its higher melting point, the titanium reinforcement could have induced a slower cooling rate, resulting in larger prior austenite grains. Larger prior austenite grains have been reported to induce acicular ferrite dominance and reduce allotriomorphic and widmanstatten ferrite growth (Bhadeshia & Honeycombe, 2006). Furthermore, titanium-rich inclusions are reported to also promote acicular ferrite formation in steel welds (Bhadeshia & Honeycombe Robert, 2006). In the HAZ the microstructures are similar. Widmanstatten ferrite grows dominantly across the coarse prior austenite grains, while sections of degenerate pearlite are observable in both reinforced and unreinforced samples (Fig. 11). These coarse grains in the HAZ correlate with the lower hardness values typically obtained in this region as depicted in Fig. 8.

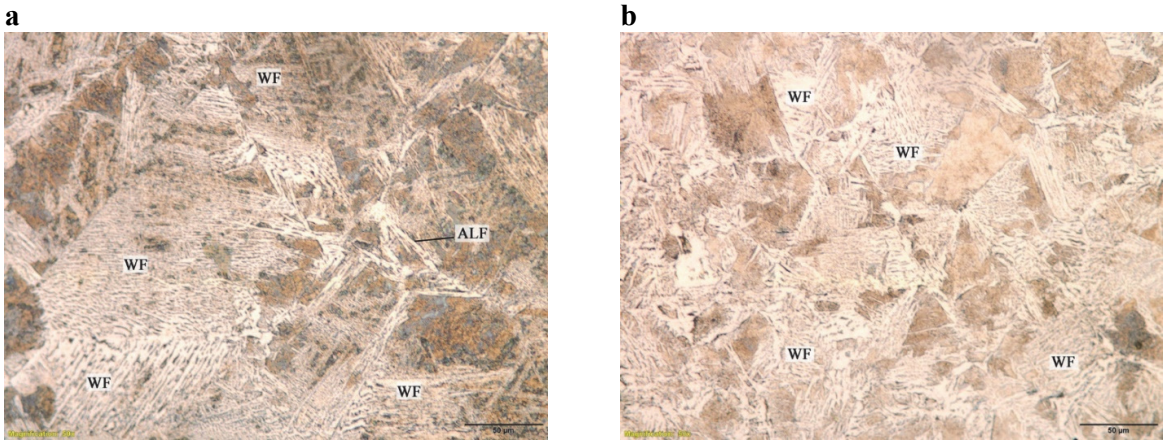

Fig. 11. Micrographs of the HAZ of (a) Unreinforced sample (b) Reinforced sample

3.2.4 EDS and XRD Analysis

In order to confirm the mixing of the titanium alloy reinforcement in the weld region, an energy dispersion spectroscopy analysis was carried out using a TESCAN SEM installed with EDS. This analysis reveals the elemental composition of carefully chosen areas of focus in the WM of the samples. Fig. 12 shows the elemental composition of an area (Fig. 12a) in the reinforced sample. As can be observed from Fig. 12b-c, Ti is sufficiently distributed in the weld zone with a weight percentage of 0.06 %. The low weight percentage indicates a small volume fraction of powder present at the weld zone in the selected area.

a

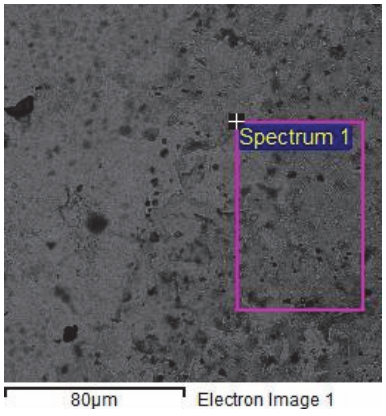

b

Element	Weight%	Atomic%
N K	0.43	1.27
O K	13.84	35.41
Si K	0.62	0.91
Ti K	0.06	0.05
Mn K	1.17	0.88
Fe K	83.87	61.49
Totals	100.00	

c

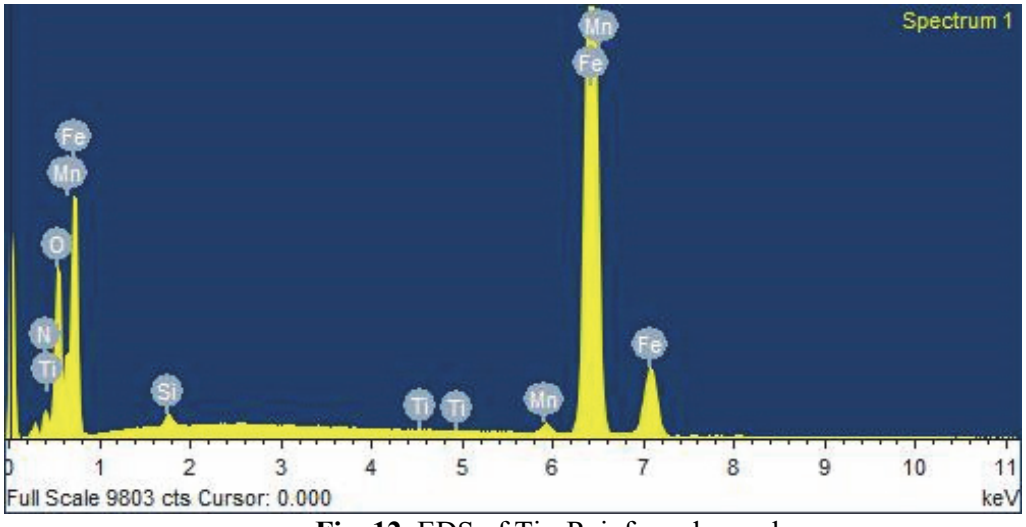

Fig. 12. EDS of Ti - Reinforced sample.

X-ray diffraction was also carried out on the welded samples to indicate the crystalline phases present in the weld zone and the spectra are given in Fig. **13**a-b for the reinforced and unreinforced samples respectively. Table 8 presents the identified phase names, their chemical formulae and weight percentage. In the unreinforced samples, α-Fe diffracts at 44.6º, 65.1º and 82.3º, with the most intense diffraction occurring at 44.6º. This is in contrast with the reinforced sample where intermetallic iron-titanium compounds diffract strongly at 44.4º and less so at 64.7º and 82.1º. Martensite with a suspected chemical formula of $C_{0.12}Fe_{1.88}$ is also observed at 44.4º and 64.7º diffraction angles. However, martensite was not identified in the WM during optical microscopy. Nevertheless, it is not unusual that martensite could be present in the WM of welded mild steel in microphases (Bhadeshia, H. K. D. H & Honeycombe Robert, 2006; Nathan et al., 2015). Intermetallic compounds are known to be very brittle and hard, and this could explain the higher hardness values observed in the WM region of the optimised reinforced butt joint samples shown in Fig. 8.

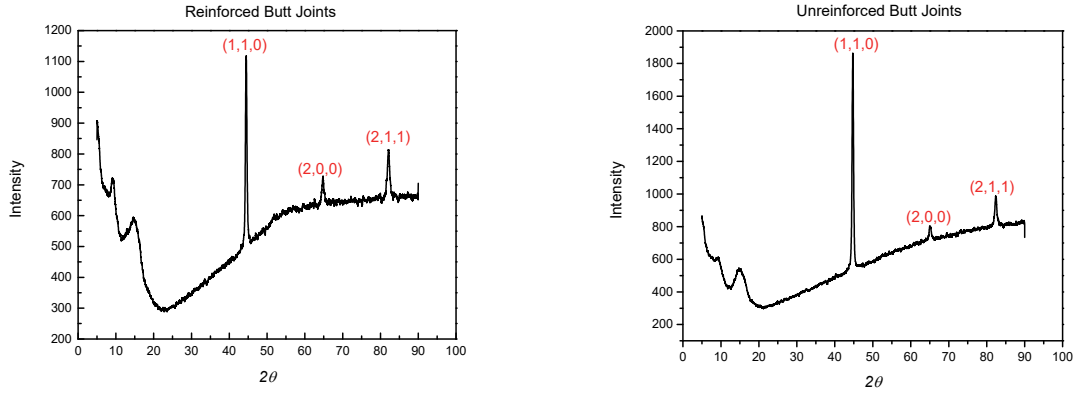

a b

Fig. 13. Diffractogram of reinforced and unreinforced butt joint samples

Table 8. Phase identification of XRD Analysis

Sample	Identified Phase	Miller Indices	Chemical Formula	Weight %
Butt Unreinforced	α-Iron	(1,1,0) (2,0,0) (2,1,1)	Fe	100.0
Butt Reinforced	Iron-Titanium	(1,1,0) (2,0,0) (2,1,1)	$Fe_{0.975}Ti_{0.025}$	81.2
	Martensite	(1,1,0) (2,0,0)	$C_{0.12}Fe_{1.88}$	18.8

3.2.5 Failure Analysis

To explain the reason for the material failure of the butt welds when subjected to tensile loading, a failure analysis using SEM and EDS was carried out on the reinforced samples. All the reinforced samples underwent failure at the base metal region. Fig. 14a shows the SEM image of the fracture region. The prevalence of Micro-void coalescence (MVC) in this region indicates a predominantly ductile mode of fracture. However, an impurity is identified at 'spectrum 1' and its spectrum, obtained via EDS is given in Fig. 14b. The elemental composition also obtained from EDS is given in Table 9. The impurity at the zone of fracture is made up of predominantly nitrogen and oxygen by weight percentage. Such impurities could be responsible for creating stress concentrations within the parent material, making that region susceptible to failure during tensile loading. This failure analysis highlights the good tensile strength of the reinforced WM region. It is noteworthy that failure did not occur in or around the reinforced weld zone. However, it remains to be seen, what the material performance will be under tensile loading if the impurities within the parent material were not as pronounced. Nevertheless, with a joint efficiency of 96.92 %, the strength of the reinforced weld in a purer parent material appears promising.

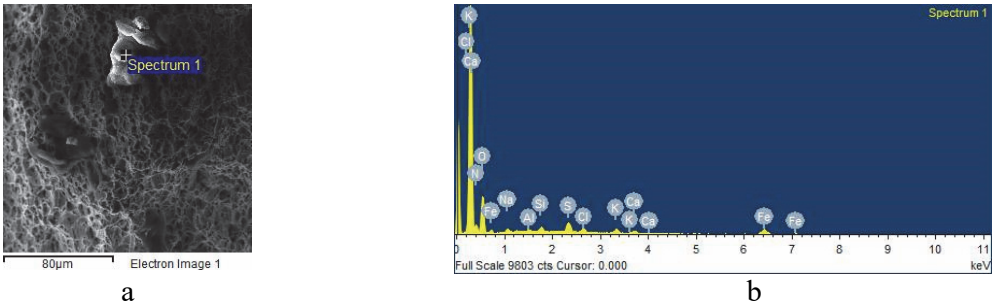

a b

Fig. 14. SEM image and EDS of fracture region of reinforced sample

Table 9. Elemental composition of impurity at spectrum 1

Element	Weight %	Atomic %
N	38.22	44.75
O	48.11	49.32
Al	0.37	0.23
Si	0.93	0.55
S	2.54	1.30
Cl	1.12	0.52
K	1.28	0.54
Ca	1.00	0.41
Fe	5.21	1.53
Na	1.20	0.86

4. Conclusions

In this study, Ti 6-2-2-2-2 reinforced mild steel butt welds have been created after an optimisation process using an L4 Orthogonal Array from Taguchi. The optimum parameters for the reinforced samples were calculated to be 24V and 215A. The reinforced butt welds were directly compared with unreinforced butt welds which were welded using the same parameters. The following deductions were made from the comparison.

1. There was no substantial improvement in the tensile strength of the butt welds due to the addition of Ti 6-2-2-2-2 alloy powder.

2. The microhardness of the reinforced butt welds was higher in the WM zone than in the WM of their unreinforced counterparts. XRD analysis revealed the presence of Titanium-Iron intermetallic compounds and suspected martensite microphases in the WM, and these could be responsible for the higher hardness values observed in the reinforced samples.

3. The study of the microstructure of the reinforced samples revealed a prevalence of acicular ferrite formation in the WM. This was attributed to the presence of Titanium inclusions in the WM. This prevalence of acicular ferrite suggests superior fracture toughness and wear resistance properties of the reinforced welds compared to their unreinforced counterparts.

4. Failure analysis of the reinforced butt welds using SEM equipped with EDS revealed that failure due to tensile loading occurred at the base metal region in an area where an impurity was present. A suspected increase in stress concentrations around these areas of impurity was a likely responsible failure in this region. This also indicates sufficient weld joint strength of the reinforced sample, as failure did not occur in the weld region despite a joint efficiency of 96.92%.

Acknowledgements

The authors would like to thank the South African Institute of Welding, Johannesburg for their support in carrying out the welding experiments at their facility.

References

Abbaschian, R., & Reed-Hill, R. E. (2008). Physical metallurgy principles Cengage Learning.

Aita, C. A. G., Goss, I. C., Rosendo, T. S., Tier, M. D., Wiedenhöft, A., & Reguly, A. (2020). Shear Strength Optimization for FSSW AA6060-T5 Joints by Taguchi and Full Factorial Design. *Journal of Materials Research and Technology, 9*(6), 16072-16079.

Akbari, M., Aliha, M. R. M., Keshavarz, S. M. E., & Bonyadi, A. (2019). Effect of tool parameters on mechanical properties, temperature, and force generation during FSW. *Proceedings of the Institution of Mechanical Engineers, Part L: Journal of Materials: Design and Applications, 233*(6), 1033-1043.

Aliha, M. R. M., & Gharehbaghi, H. (2017). The effect of combined mechanical load/welding residual stress on mixed mode fracture parameters of a thin aluminum cracked cylinder. *Engineering Fracture Mechanics, 180*, 213-228.

Aliha, M. R. M., Ghoreishi, S. M. N., Imani, D. M., Fotoohi, Y., & Berto, F. (2020). Mechanical and fracture properties of aluminium cylinders manufactured by orbital friction stir welding. *Fatigue & Fracture of Engineering Materials & Structures.*

Aliha, M. R. M., Kalantari, M. H., Ghoreishi, S. M. N., Torabi, A. R., & Etesam, S. (2019). Mixed mode I/II crack growth investigation for bi-metal FSW aluminum alloy AA7075-T6/pure copper joints. *Theoretical and Applied Fracture Mechanics, 103*, 102243.

Aliha, M. R. M., Shahheidari, M., Bisadi, M., Akbari, M., & Hossain, S. (2016). Mechanical and metallurgical properties of dissimilar AA6061-T6 and AA7277-T6 joint made by FSW technique. *The International Journal of Advanced Manufacturing Technology, 86*(9-12), 2551-2565.

Anand, K., Barik, B. K., Tamilmannan, K., & Sathiya, P. (2015). Artificial neural network modeling studies to predict the friction welding process parameters of Incoloy 800H joints. *Engineering Science and Technology, an International Journal, 18*(3), 394-407.

ASTM International. (2016). ASTM E8 / E8M-16a, standard test methods for tension testing of metallic materials. West Conshohocken, PA:

Bahrami, M., Dehghani, K., & Givi, M. K. B. (2014). A novel approach to develop aluminum matrix nano-composite employing friction stir welding technique. *Materials & Design, 53*, 217-225.

Bhadeshia, H. K. D. H, & Honeycombe Robert. (2006). *Steels: Microstructure and properties* (3rd ed.). 30 Corporate Drive, Suite 400, Burlington,MA 01803, USA: Elsevier Ltd.

Bhole, S. D., Nemade, J. B., Collins, L., & Liu, C. (2006). Effect of nickel and molybdenum additions on weld metal toughness in a submerged arc welded HSLA line-pipe steel. *Journal of Materials Processing Technology, 173*(1), 92-100.

Byung-Wook, A., Don-Hyun, C., Yong-Hwan, K., & Seung-Boo, J. (2012). Fabrication of SiCp/AA5083 composite via friction stir welding. *Transactions of Nonferrous Metals Society of China, 22*, s634-s638.

da Trindade Filho, V B, Guimaraes, A. S., Payao Filho, J da C, & Paranhos, R. d. R. (2004). Normalizing heat treatment effect on low alloy steel weld metals. *Journal of the Brazilian Society of Mechanical Sciences and Engineering, 26*(1), 62-66.

Eslami, N., Hischer, Y., Harms, A., Lauterbach, D., & Böhm, S. (2019). Optimization of process parameters for friction stir welding of aluminum and copper using the taguchi method. *Metals, 9*(1), 63.

Fattahi, M., Mohammady, M., Sajjadi, N., Honarmand, M., Fattahi, Y., & Akhavan, S. (2015). Effect of TiC nanoparticles on the microstructure and mechanical properties of gas tungsten arc welded aluminum joints. *Journal of Materials Processing Technology, 217*, 21-29.

Gharibshahiyan, E., Raouf, A. H., Parvin, N., & Rahimian, M. (2011). The effect of microstructure on hardness and toughness of low carbon welded steel using inert gas welding. *Materials & Design, 32*(4), 2042-2048.

Hooda, A., Dhingra, A., & Sharma, S. (2012). Optimization of MIG welding process parameters to predict maximum yield strength in AISI 1040. *International Journal of Mechanical Engineering and Robotics Research, 1*(3).

Jacques, L., & El Ouafi, A. (2018). ANN based predictive modelling of weld shape and dimensions in laser welding of galvanized steel in butt joint configurations. *Journal of Minerals and Materials Characterization and Engineering, 6*(03), 316.

Lacki, P., & Derlatka, A. (2017). Strength evaluation of beam made of the aluminum 6061-T6 and titanium grade 5 alloys sheets joined by RFSSW and RSW. *Composite Structures, 159*, 491-497.

Kazi, J., Zaid, S., Talha, S. M., Yasir, M., & Akib, D. (2015). A review on various welding techniques. *International Journal of Modern Research, 5*(2), 22-28.

Kumar, P., Dhingra, A. K., & Kumar, P. (2016). Optimization of process parameters for machining of mild steel EN18 by response surface methodology. *Advances in Engineering: An International Journal, 1*, 1-12.

Mirjavadi, S. S., Alipour, M., Emamian, S., Kord, S., Hamouda, A., Koppad, P. G., & Keshavamurthy, R. (2017). Influence of TiO2 nanoparticles incorporation to friction stir welded 5083 aluminum alloy on the microstructure, mechanical properties and wear resistance. *Journal of Alloys and Compounds, 712*, 795-803.

Mirzaei, M., Jeshvaghani, R. A., Yazdipour, A., & Zangeneh-Madar, K. (2013). Study of welding velocity and pulse frequency on microstructure and mechanical properties of pulsed gas metal arc welded high strength low alloy steel. *Materials & Design, 51*, 709-713.

Mohammad Aliha, M. R., Fotouhi, Y., & Berto, F. (2018). Experimental notched fracture resistance study for the interface of Al–Cu bimetal joints welded by friction stir welding. *Proceedings of the Institution of Mechanical Engineers, Part B: Journal of Engineering Manufacture, 232*(12), 2192-2200.

Narasimharaju, S., & Sankunny, S. (2019). Microstructure and fracture behavior of friction stir lap welding of dissimilar AA 6060-T5/pure copper. *Engineering Solid Mechanics, 7*(3), 217-228.

Narendranath, S., & Chakradhar, D. (2018). Process parameter optimization for FSW of AA6061/SiC/fly ash AMCs using Taguchi technique. *Emerging Materials Research, 7*(3), 192-199.

Nathan, S. R., Balasubramanian, V., Malarvizhi, S., & Rao, A. G. (2015). Effect of welding processes on mechanical and microstructural characteristics of high strength low alloy naval grade steel joints. *Defence Technology, 11*(3), 308-317.

Odiaka, T., Madushele, N., & Akinlabi, S. (2018). (2018). Improvement of joint integrity in MIG welded steel: A review. *Paper presented at the ASME 2018 International Mechanical Engineering Congress and Exposition,*

Olabi, A. G., Casalino, G., Benyounis, K. Y., & Hashmi, M. S. J. (2006). An ANN and Taguchi algorithms integrated approach to the optimization of CO2 laser welding. *Advances in Engineering Software, 37*(10), 643-648.

Owunna, I., & Ikpe, A. E. (2019). Modelling and prediction of the mechanical properties of TIG welded joint for AISI 4130 low carbon steel plates using Artificial Neural Network (ANN) approach. *Nigerian Journal of Technology, 38*(1), 117-126.

Paidar, M., Asgari, A., Ojo, O. O., & Saberi, A. (2018). Mechanical properties and wear behavior of AA5182/WC nanocomposite fabricated by friction stir welding at different tool traverse speeds. *Journal of Materials Engineering and Performance, 27*(4), 1714-1724.

Pal, A. (2015). MIG welding parametric optimisation using taguchi's orthogonal array and analysis of variance. *International Journal of Research Review in Engineering Science and Technology, 4*(1), 211-217.

Paniagua-Mercado, A. M., Lopez-Hirata, V. M., Dorantes-Rosales, H. J., Diaz, P. E., & Valdez, E. D. (2009). Effect of TiO2-containing fluxes on the mechanical properties and microstructure in submerged-arc weld steels. *Materials Characterization, 60*(1), 36-39.

Pantelis, D. I., Karakizis, P. N., Daniolos, N. M., Charitidis, C. A., Koumoulos, E. P., & Dragatogiannis, D. A. (2016). Microstructural study and mechanical properties of dissimilar friction stir welded AA5083-H111 and AA6082-T6 reinforced with SiC nanoparticles. *Materials and Manufacturing Processes, 31*(3), 264-274.

Rakesh, S. K. (2014). Determination of significant process parameter in metal inert gas welding of mild steel by using analysis of variance (ANOVA). *International Journal of Engineering and Management Research, 4*(2), 271-276.

Ramakrishna, G., Rao, P. S., & Rao, P. G. (2016). Methods to improve mechanical properties of welded joints: View point. *International Journal of Mechanical Engineering and Technology, 7*(6), 309-314.

Sapakal, S. V., & Telsang, M. T. (2012). Parametric optimization of MIG welding using taguchi design method. *International Journal of Advabced Engineering Resource Studies, 1*(4), 28-30.

Sevim, I., & Eryurek, I. B. (2006). Effect of abrasive particle size on wear resistance in steels. *Materials & Design, 27*(3), 173-181.

Shojaeefard, M. H., Akbari, M., Khalkhali, A., Asadi, P., & Parivar, A. H. (2014). Optimization of microstructural and mechanical properties of friction stir welding using the cellular automaton and Taguchi method. *Materials & Design, 64*, 660-666.

Singh, B., Khan, Z. A., Siddiquee, A. N., & Maheshwari, S. (2016). Effect of CaF2, FeMn and NiO additions on impact strength and hardness in submerged arc welding using developed agglomerated fluxes. *Journal of Alloys and Compounds, 667*, 158-169.

Singh, V. (2013). An investigation for gas metal arc welding optimum parameters of mild steel AISI 1016 using taguchi‟ s method. *International Journal of Engineering and Advanced Technology (IJEAT), 2*(6), 407-409.

Sivagurumanikandan, N., Saravanan, S., Kumar, G. S., Raju, S., & Raghukandan, K. (2018). Prediction and optimization of process parameters to enhance the tensile strength of Nd: YAG laser welded super duplex stainless steel. *Optik, 157*, 833-840.

Srivastava, S., & Garg, R. K. (2017). Process parameter optimization of gas metal arc welding on IS:2062 mild steel using response surface methodology

Taheri-Behrooz, F., Aliha, M. R., Maroofi, M., & Hadizadeh, V. (2018). Residual stresses measurement in the butt joint welded metals using FSW and TIG methods. *Steel and Composite Structures, 28*(6), 759-766.

Torabi, A. R., Kalantari, M. H., & Aliha, M. R. M. (2018). Fracture analysis of dissimilar Al-Al friction stir welded joints under tensile/shear loading. *Fatigue & Fracture of Engineering Materials & Structures, 41*(9), 2040-2053.

Utkarsh, S., Neel, P., Mahajan, M. T., Jignesh, P., & Prajapati, R. B. (2014). Experimental investigation of MIG welding for ST-37 using design of experiment. *International Journal of Scientific and Research Publications, 4*(5), 1.

Yuvaraj, N., & Aravindan, S. (2015). Fabrication of Al5083/B4C surface composite by friction stir processing and its tribological characterization. *Journal of Materials Research and Technology, 4*(4), 398-410.

Zhao, D., Ren, D., Zhao, K., Pan, S., & Guo, X. (2017). Effect of welding parameters on tensile strength of ultrasonic spot welded joints of aluminum to steel–By experimentation and artificial neural network. *Journal of Manufacturing processes, 30*, 63-74.